EPJ Web of Conferences **146**, 11010 (2017) DOI: 10.1051/epjconf/201714611010
ND2016

^{10}B(n,α)^{7}Li and ^{10}B(n,$\alpha_1\gamma$)^{7}Li cross section data up to 3 MeV incident neutron energy

Riccardo Bevilacqua[1,a], Franz-Josef Hambsch[2,b], Marzio Vidali[2], Ivan Ruskov[3], and Livio Lamia[4]

[1] European Spallation Source ERIC, Lund, Sweden
[2] EC-JRC-Directorate G, Unit G.2, Geel, Belgium
[3] Institute for Nuclear Research and Nuclear Energy, Sofia, Bulgaria
[4] Laboratori Nazionali del Sud, Istituto Nazionale di Fisica Nucleare, Catania, Italy

Abstract. The ^{10}B(n,α) reaction cross-section is a well-established neutron cross-section standard for incident neutron energies up to 1 MeV. However, above this energy limit there are only scarce direct (n,α) measurements available and these few experimental data are showing large inconsistencies with each other. These discrepancies are reflected in the evaluated data libraries: ENDF/B-VII.1, JEFF-3.1.2 and JENDL-4.0 are in excellent agreement up to 100 keV incident neutrons, whereas the ^{10}B(n,α) data in the different libraries show large differences in the MeV region. To address these inconsistencies, we have measured the cross section of the two branches of the ^{10}B(n,α) reaction for incident neutron energies up to 3 MeV. We present here the ^{10}B(n,α) and the ^{10}B(n,$\alpha_1\gamma$) reactions cross section data, their branching ratio and the total ^{10}B(n,α) reaction cross section. The measurements were conducted with a dedicated Frisch-grid ionization chamber installed at the GELINA pulsed neutron source of the EC-JRC. We compare our results with existing experimental data and evaluations.

1. Introduction

The ^{10}B(n,α)^{7}Li, the ^{10}B(n,$\alpha_1\gamma$)^{7}Li reaction cross-section data are used as standard references in the measurement and evaluation of other neutron reaction cross sections [1]. Moreover, these reaction data are important for a wide range of applications, including nuclear safety, security and safeguards, non-proliferation, stockpile stewardship, and more.

Data for the ^{10}B(n,α)^{7}Li, the ^{10}B(n,$\alpha_1\gamma$)^{7}Li reactions are included in the ENDF/B-VII evaluated library as cross section standards for neutron energies from thermal up to 1 MeV. However, above this energy limit, large discrepancies emerge in different evaluated data libraries (Fig. 1), and available experimental data offer no conclusive results [1].

The European Commission's Joint Research Centre has joined an international effort to extend the ^{10}B(n,α)^{7}Li, the ^{10}B(n,$\alpha_1\gamma$)^{7}Li reactions cross section's status as standard to the MeV region. To measure these reactions and provide benchmark data, three experimental setups, consisting of dedicated Frisch-grid ionization chambers, have been installed and operated at the Geel Linear Accelerator (GELINA) pulsed neutron time-of-flight (TOF) facility and at the 7 MV Van de Graaff (VDG) facility [2].

These measurements will provide cross section data for incident neutron energies up to 3 MeV. Here are presented the experimental methods used at GELINA to measure these reactions, results for the ^{10}B(n,α_0)/^{10}B(n,$\alpha_1\gamma$) branching ratio, cross sections for the ^{10}B(n,α)^{7}Li reaction and for its two reaction branches. The incident neutron energy is covered from ~100 keV to 3 MeV.

2. Experimental setups at GELINA

A double Twin Frisch-Grid Ionization Chamber (TFGIC) was installed at the flight path station FP16/60 of the GELINA facility, at a distance of 60 m from the neutron production target. At this flight path, an unmoderated neutron beam is available.

The TOF technique was used for the neutron energy (E_n) determination. The TOF-to-E_n calibration was obtained by the position of the γ-flash; the repetition rate of the pulsed neutron beam was 800 Hz. Here, the α particle production from the ^{10}B(n,α_0)^{7}Li and the ^{10}B(n,$\alpha_1\gamma$)^{7}Li reaction, was measured for E_n up to 3 MeV.

This TFGIC is an upgrade to the single TFGIC used in Ref. [3]; two chambers have been connected in order to install two boron reaction targets, coupled back-to-back with two ^{235}U reaction targets. This configuration allowed the cross section measurement by normalization to the ^{235}U(n,f) standard. The electronic chain was the same as described in Ref. [3].

The boron targets consisted of two 84 mm-diameter deposits of ^{10}B (98.3% purity, 94.0% enriched), respectively 14.5 (±0.8) μg/cm^2 and 15.7 (±0.8) μg/cm^2, on polished stainless steel backings; the ^{10}B mass was determined by differential weighing [3]. The uranium targets consisted of two 45 mm-diameter deposits of $^{235}UF_4$ (97.663(±0.003)% enriched) on aluminum backings. The deposited uranium mass was determined by low-geometry α counting, and it was respectively 3081 (±46) μg

[a] e-mail: Riccardo.Bevilacqua@esss.se
[b] e-mail: Franz-Josef.Hambsch@ec.europa.eu

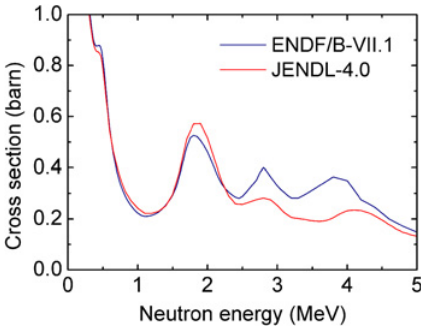

Figure 1. Evaluated cross sections for the ^{10}B(n,α)^{7}Li reactions for neutron energies up to 5 MeV. The ENDF/B-VII.1 data represent the present standard up to 1 MeV [1]. Clear discrepancies exists between the ENDF/B-VII.1 evaluation and other evaluated data libraries.

and 3071 ($\pm$46) μg, corresponding to a thickness of 193.7 ($\pm$2.9) μg/cm^2 and 193.1 ($\pm$2.9) μg/cm^2.

3. Results

3.1. Data reduction and analysis

Anode and Sum (Anode + Grid) amplitudes were stored event-by-event in a listmode file, along with the time information from a time coder. A common trigger was set for the four half-chambers of the TFGIC, hence for each triggering event, all signals from the chamber were recorded and stored at the same moment.

The first step of the analysis consisted in reading the listmode files, with the GENDARC code developed at JRC, and converting them in Root TTrees. The time information was reconstructed and the incident neutron energy calculated relativistically for each event. The neutron energy calibration was obtained using the gamma-flash position and known resonances. Data were then corrected for electronic shift and grid inefficiency. Energy calibration of the anode signal was obtained from Kinematics [4] and SRIM calculations [5]. The angular information was firstly determined in the laboratory system (LAB), and then converted in the center-of-mass system (CMS) by means of relativistic equations. At the same time, the emission energy was calculated in the CMS.

Since the relationship between α particle emission energy and the incident neutron energy is linear in the CMS, it is possible to define a *thermal-equivalent* energy: subtracting the momentum transfer from the emission energy in the CMS, the α_0 and the α_1 line will be respectively at 1.78 MeV and 1.47 MeV. This transformation allows an improved separation of the α lines in the neutron energy region of interest, as shown in Fig. 2, compared to e.g., in the CMS.

3.2. Angular distributions

Angular distributions for the α particle emission in the CMS are important for theoretical R-matrix calculations. They would allow to determine double differential cross sections (in energy and in emission angle), however the statistics is the limiting factor. Angular distributions allow also to correct the data for the Particle Leaking effect [6] via Legendre polynomial fitting [7].

In Fig. 3, the two-dimensional angular distribution of the events induced by 1200 ($\pm$50) keV neutrons, in the forward hemisphere in the LAB are shown. Whereas the angular distribution is the same in both the CMS and the thermal-equivalent system, the separation of the two α lines is better in the latter. The Li + α group corresponds to Particle Leaking events, when both reaction products are emitted forward in the LAB. The α lines are fitted by two Gaussian distributions; the events in a 3 σ interval around the respective distribution's mean are selected and identified as α_0 or α_1.

The TFGIC is affected by a detection limit at large emission angles $\cos_{LAB}(\theta)\sim 0$ due to energy and particle losses in the ^{10}B deposition. Moreover the Particle Leaking effect [6] suppresses the identification of the α particles in an angular interval dependent on the incident neutron energy. To account for these missing events, the measured angular distributions were fitted with Legendre polynomials, following the method described in Ref. [7].

3.3. Branching ratio ^{10}B(n,α_0)/^{10}B(n,$\alpha_1\gamma$)

The branching ratio ^{10}B(n,α_0)/^{10}B(n,$\alpha_1\gamma$) is defined as the ratio of the α_0 and the α_1 yield, for a given neutron energy.

Since it represents the relative probability of the two reactions, the branching ratio is a function of the incident neutron energy, but it is independent from the shape of the neutron energy spectrum. Hence, the ratio of the reaction yields is exactly the same as the ratio of the ^{10}B(n,α_0) and of the ^{10}B(n,$\alpha_1\gamma$) reaction cross sections.

In Fig. 4, results from the present work are plotted together with evaluated and experimental data. Present data show a disagreement with previous measurements conducted at JRC-Geel [3,7], for neutron energies below 1 MeV: whereas the former are in better agreement with the JENDL-4.0 evaluation, the latter follow the ENDF and Zhenpeng evaluations. Both set of data were measured with a TFGIC and similar experimental conditions at GELINA, the main difference being that the present data were measured at 60 meters from the neutron production target and the previous data at 30 meters. However, this difference does not seem to justify the observed discrepancy.

3.4. ^{10}B(n,α_0) and ^{10}B(n,$\alpha_1\gamma$) cross sections

In Fig. 5, preliminary cross sections for the ^{10}B(n,α_0) and the ^{10}B(n,$\alpha_1\gamma$) reaction are plotted with evaluated and experimental data. There is no consistent agreement with any evaluation or previous experimental results over all the incident neutron energy spectrum. However, no previous set of experimental data shows a consistent agreement with evaluated data either. The α_0 data are in agreement with ENDF from 0.5 to 1.25 MeV and from 1.6 to 1.7 MeV, whereas above this limit they are consistently lower than the evaluations and in good agreement with Davis data.

The situation is more complex when comparing the α_1 data: the results are in good agreement with Davis [8] data from 0.4 to 1.3 MeV and from 1.6 to 2.6 MeV, whereas the agreement with either ENDF and JENDL is not consistent over all the measured energy spectrum. From 0.4 to 1.0 MeV present α_1 data are in agreement with both

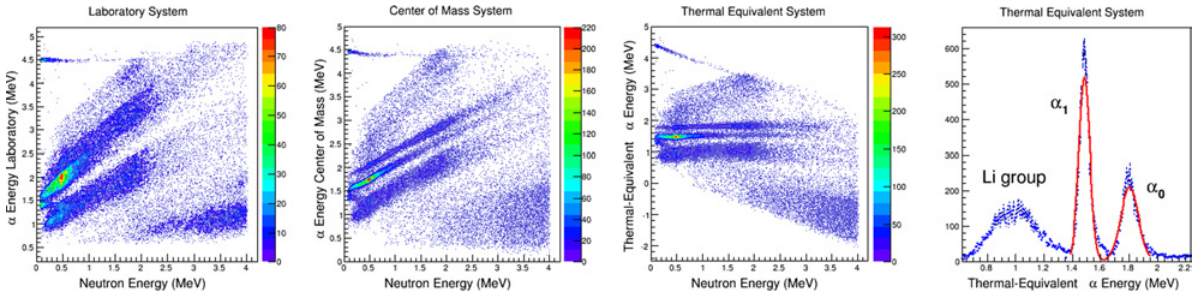

Figure 2. α particle emission energy as a function of the incident neutron energy in the LAB (first panel), in the CMS (second panel) and in the thermal-equivalent system (third panel). In the fourth panel, data are projected on the thermal-equivalent axis and it is possible to observe that the two α lines are well separated; red lines are Gaussian fittings of the experimental distributions. Plotted data include all incident neutron energies from 80 keV to 4 MeV, in the LAB forward hemisphere.

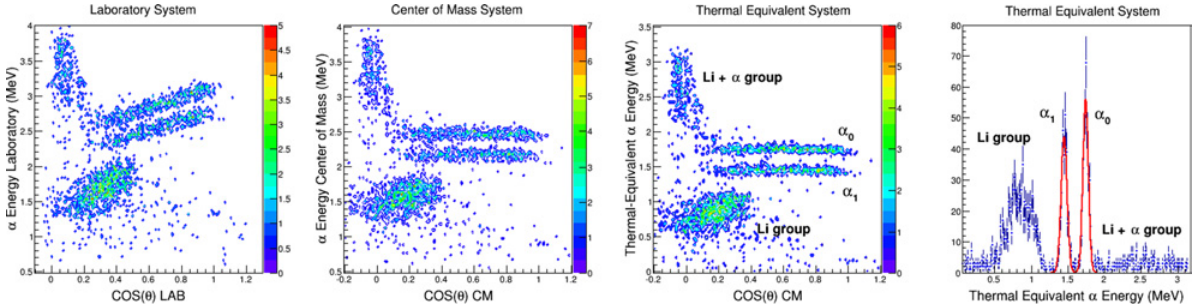

Figure 3. α particle emission energy as a function of the angular distribution in the LAB (first panel), in the CMS (second panel) and in the thermal-equivalent system (third panel). In the fourth panel, data are projected on the thermal-equivalent axis to observe well separated α lines; red lines are Gaussian fittings of the experimental distributions. Data shown are at $E_n = 1200\ (\pm 50)$ keV, in the LAB forward hemisphere.

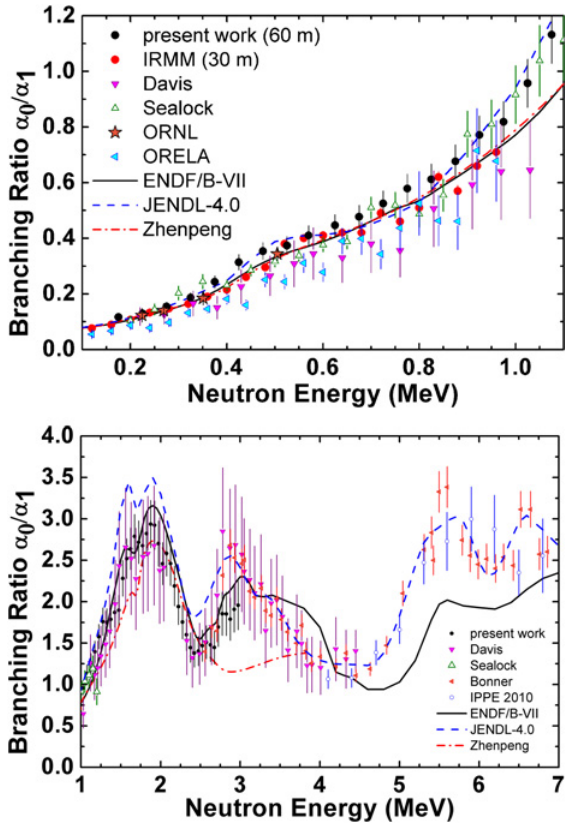

Figure 4. ^{10}B(n,α_0)/^{10}B(n,$\alpha_1\gamma$) branching ratio in comparison with evaluated and experimental data [3,8–12], for 0.1 to 1.1 MeV (upper panel) and for 1.0 to 7.0 MeV (lower panel) incident neutron energies.

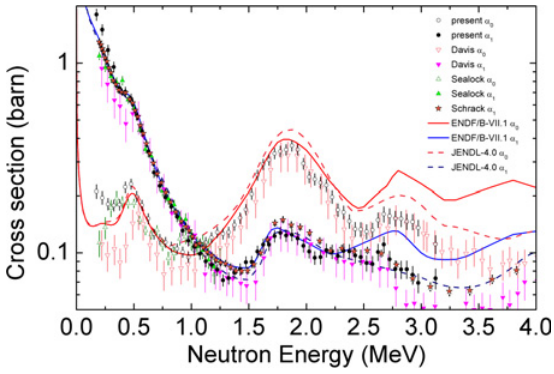

Figure 5. ^{10}B(n,α_0) and ^{10}B(n,$\alpha_1\gamma$) reaction cross sections for neutron energies from 0.1 to 4.0 MeV, in comparison with evaluated and experimental data [8,9,13].

evaluations and other experimental data. However, when at 1 MeV a difference emerge between ENDF and JENDL, the present results first follow JENDL, in agreement with Davis, then above 1 MeV our results start to follow ENDF, in agreement with Schrack [13]. Above 1.6 MeV our data are again in agreement with Davis and the evaluations, with some difference around 2.1 MeV. From 2.2 MeV our data are in agreement with Schrack again, following mostly the JENDL evaluation (but for a structure around 2.6 MeV).

Present cross sections for both α_0 and α_1 are higher than evaluations and previous data below 0.4 MeV: this discrepancy might indicate a background problem in the α data as well as in the ^{235}U(n,f) counts.

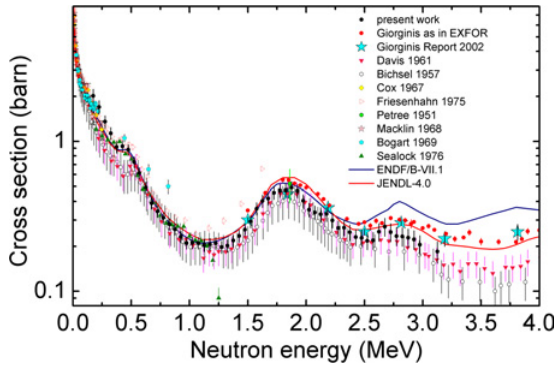

Figure 6. ^{10}B(n,α)^{7}Li cross section for neutron energies from 0.1 to 4.0 MeV, in comparison with evaluated and experimental data [6,8,9,14,16–21].

3.5. ^{10}B(n,α)^{7}Li cross sections

Preliminary results for the total cross section of the ^{10}B(n,α)^{7}Li reaction are plotted in Fig. 6. The total cross section is obtained from the sum of the partial α_0 and α_1 cross sections presented in the previous section, and it is dominated by α_0 below 1.1 MeV and by α_1 above this limit.

The present data are in statistical agreement with Davis [8] and Bichsel [16] data over all the energy spectrum, however the present cross sections are mostly higher than both other sets. However, data from Ref. [6], measured at the JRC-Geel Van de Graaff, are consistently higher than our results. A possible explanation is the use of a different method to determine the total number of events, which is sensitive to anisotropies in the angular distribution of the emitted α particles [6,14,15].

4. Conclusions

The ^{10}B(n,α)^{7}Li, the ^{10}B(n,$\alpha_1\gamma$)^{7}Li reaction cross-section as well as the toal cross section ^{10}B(n,α) have been determined in the energy range from say 500 keV to 3 MeV. Below 500 keV obvious problems with background have been observed, however the results above that limit have been identified as trustworthy. The anlysis has been done to the best of our knowlegde. No further experiments are planned.

References

[1] International Atomic Energy Agency, International evaluation of neutron cross-section standards, ISBN: 92-0-100807-4 (2007)
[2] R. Bevilacqua et al., Nuclear Data Sheet **119**, 104 (2014)
[3] F.-J. Hambsch et al., Nucl. Sci. Eng. **156**, 103–114 (2007)
[4] G. Lövestam, Kinematics – a program for calculation of nuclear reaction kinematics, EC-JRC-IRMM (2007)
[5] J.F. Ziegler et al., Nucl. Inst. Meth. B **268**, 1818 (2010)
[6] G. Giorginis et al., Nucl. Inst. Meth. A **538**, 550 (2005)
[7] F.-J. Hambsch et al., Nucl. Sci. Eng. **163**, 1 (2009)
[8] Davis et al., Nuclear Physics **27**, 448 (1961)
[9] R.M. Sealock et al., Phys. Rev. C **13**, 2149 (1976)
[10] R.L. Macklin et al., Phys. Rev. **165**, 1147 (1968)
[11] L.W. Weston and J.H. Todd et al., Nucl. Sci. Eng. **109**, 113 (1991)
[12] V.A. Khryachkov et al., EPJ Web of Conferences **21**, 03005 (2012)
[13] R.A. Schrack et al., Nucl. Sci. Eng. **114**, 352 (1993)
[14] G. Giorginis and V. Khryachkov, EC-JRC-IRMM Nuclear Physics Unit, GER/NP/2002/05/30 (2002)
[15] G. Giorginis and V. Khryachkov, EC-JRC-IRMM Nuclear Physics Unit, EUR 21017 EN, 61–64 (2003)
[16] H. Bichsel and T.W. Bonner, Phys. Rev. **108**, 1025 (1957)
[17] S.A. Cox and F.R. Pontet, J. Nucl. Ener. **21**, 271 (1967)
[18] S.J. Friesenhahn et al., Conf. on Nucl. Cross-Sect. and Techn., Washington Vol. 1, p. 232 (1975)
[19] B. Petree et al., Phys. Rev. **83**, 1148 (1951) as reported by Davis (1961)
[20] R.L. Macklin and J.H. Gibbons, Phys. Rev. **165**, 1147 (1968)
[21] D. Bogart and L.L. Nichols, Nucl. Phys. A **125**, 463 (1969)